Theoretical Studies on Structures and Spectroscopic Properties of Self-Assembled Bis(2,4,8,10-tetramethyl-9-methoxycarbonylethyldipyrrin-3-yl)methane with Co(II)

Wei Li,*,† Feng Yang,† Zengdong Wang,† Jiming Hu,*,‡ and Jinshi Ma§

Department of Chemical Engineering, Wuhan University of Science and Engineering, Wuhan 430073, China, College of Chemistry and Molecular Science, Wuhan University, Wuhan 430072, China, and CAS Key Laboratory of Photochemistry, Institute of Chemistry, Chinese Academy of Sciences, Beijing 100080, China

Received: October 5, 2008; Revised Manuscript Received: February 4, 2009

We report a combined experimental and computational study of the large self-assembly complex $(CoL)_2$ [L= bis(2,4,8,10-tetramethyl-9-methoxycarbonylethyldipyrrin-3-yl)methane] containing 172 atoms. An extensive density functional theory (DFT) and time-dependent DFT study of this complex in gas phase and in CH_2Cl_2 solution was performed, investigating the effect of substitutions of methyl and methyl propionate on the electronic structure and optical properties of this complex. The calculated IR and Raman spectra are in excellent agreement with the experiment, thus allowing a detailed assignment of the vibrational absorption bands. Comparing the vibrational spectrum of $(CoL)_2$ with that of $(ZnL')_2$ [L′ = bis(2,4-dimethyldipyrrin-3-yl)methane], the substitution of methyl on the C_β atom results in sizable shifts on the same modes; particularly in the case of mode $\upsilon(C_\beta-C_\beta)$, the shift is more than 20 cm^{-1}. The lowest 70 singlet−singlet spin-allowed excited states were taken into account for the calculation by TDDFT in gas phase and PCM-TDDFT in CH_2Cl_2 solution. Theoretical calculations provide a good description on positions of the two band maximums in observed spectrum but predict a contrary relatively intensity for these two bands. In the UV−vis absorption spectrum of $(CoL)_2$ complex, the band maximum at 525.5 nm is mainly attributed to the $\pi\rightarrow\pi^*$ transition. The band maximum at 488.1 nm is originated from metal−ligand charge-transfer (MLCT) transition mixed with interligand $\pi\rightarrow\pi^*$ transition.

Introduction

Metal ion mediated self-assembly is one of most powerful approaches to supramolecular architectures. This strategy typically utilizes metal−ligand interactions to organize small molecules into large assemblies. Among many ligands designed by chemists, the polybipyridine ligands developed by Lehn and his colleagues are particularly interesting with respect to their ability to generate helicates,[1] grids,[2] cages,[3] ladders,[4] and rings.[5] In contrast to bipyridine, dipyrrin (dipyrromethenes) was recently found to be an ideal building block for supramolecular self-assembly. Dipyrrins, consisting of two pyrroles with a sp^2-meso position, are typical π-conjugated bidentate monoanionic ligands for metal ions in natural and artificial systems. Therefore, dipyrrins are promising planar scaffoldings for self-assemblies[6−11] and will give neutral coordination oligomers, which, in combination with various spacer units, can be used to fabricate fine-tuned nanoscale morphologies using bridging metal cations.[12] By varying the bridge spacers between two dipyrrin units, the self-assembly of the corresponding bis(dipyrrin) ligands with metal ion give supramolecules with different geometric shapes.[13−17] Excited-state energy transfer dynamics in self-assembled triads composed of two porphyrins and an intervening bis(dipyrrinato) metal complex[18] or composed of boron dipyrrin, zinc porphyrin, and fullerene[19] were explored. However, theoretical studies on the structure and spectroscopic properties for these kinds of large self-assembly complexes have rarely been reported.

The self-assembly complex of bis(2,4,8,10-tetramethyl-9-methoxycarbonylethyldipyrrin-3-yl)methane with Co(II) [$(CoL)_2$] contains 172 atoms. Thus, it is exceedingly difficult to develop accurate force fields for molecules of such size on a purely empirical basis. Quantum mechanical calculations of force constants can solve the difficulties of empirical force field determination by making available independent information, which is largely complementary to the spectroscopic measurements. As an economical and effective way of including electron correlation in the ground-state wave function, gradient-corrected density functional theory (DFT) is about as inexpensive as Hartree−Fock theory and is much more accurate for molecules composed of first-row atoms. Wong[20,21] has shown that the Becke−Lee−Yang three-parameter hybrid functional (B3LYP) yields remarkably accurate vibrational frequencies.

TDDFT calculations of electronic transitions are based on the response of the ground-state electron density to the oscillating optical field. The use of the ground-state density makes the question of the validity of the Hohenberg−Kohn theorems to excited states irrelevant. Therefore, TDDFT is, in principle, applicable to all excited states, regardless their spin and symmetry. For a closed-shell molecule, TDDFT can be used to calculate the whole manifolds of singlet as well as triplet excited states, provided that the transition energies are smaller than the vertical ionization potential.[22] TDDFT has emerged as a reliable standard tool for the theoretical treatment of electronic excitation spectra, and recent works demonstrate the good accuracy for a wide range of systems.[22−28] In the present study, the FT-IR and Raman spectrum of $(CoL)_2$ was recorded and theoretical computations on the geometry, electronic structure, and vibra-

* Corresponding authors. W.L.: fax, +86-027-81924375; e-mail: liwei_wuse@yahoo.com.cn. J.-M.H.: fax, +86-027-68754067; e-mail, jmhu@whu.edu.cn.

† Wuhan University of Science and Engineering.

‡ Wuhan University.

§ Chinese Academy of Sciences.

10.1021/jp808793s CCC: $40.75
Published on Web 03/06/2009

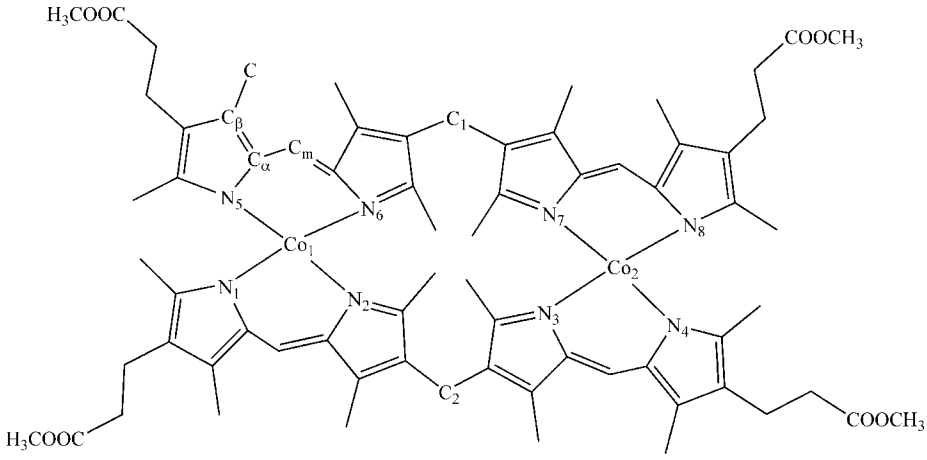

Figure 1. Chemical structure and abbreviated notation of $(CoL)_2$.

TABLE 1: Experimental (by X-ray)[17] and Optimized Geometrical Parameters (bond lengths in angstroms and bond angles in degree) of Complex $(CoL)_2$ under C_1 Symmetry in the Gas Phase with Different Basis Sets[a]

bonds	BS1	BS2	BS3	experimental	bond	BS1	BS2	BS3	experimental
Co1−N1	1.911	1.949	1.948	1.984(4)	N5−Co1−N6	94.1	93.7	93.6	95.68(18)
Co1−N2	1.909	1.938	1.937	1.981(4)	N2−Co1−N6	103.2	103.7	103.8	109.43(19)
Co1−N5	1.921	1.920	1.918	1.975(5)	N5−Co1−N1	106.6	106.2	106.5	116.16(19)
Co1−N6	1.904	1.925	1.923	1.981(4)	N2−Co1−N1	94.1	93.7	93.6	95.75(19)
Co2−N3	1.907	1.922	1.920	1.964(5)	N6−Co1−N1	143.6	145.9	145.6	122.34(18)
Co2−N4	1.912	1.940	1.920	1.967(5)	N3−Co2−N4	94.3	93.8	93.7	96.07(19)
Co2−N7	1.911	1.939	1.939	1.985(4)	N3−Co2−N8	116.1	112.9	113.1	118.15(19)
Co2−N8	1.907	1.922	1.938	1.968(5)	N4−Co2−N8	103.9	104.0	104.1	117.4(2)
Co1−Co2	7.746	7.872	7.862	7.981	N3−Co2−N7	103.8	103.9	104.2	109.67(19)
C1−C2	7.841	7.865	7.842	7.819	N8−Co2−N7	94.2	93.8	93.7	95.34(18)
N5−Co1−N2	116.6	113.2	113.5	119.11(19)	N4−Co2−N7	145.5	147.6	147.4	121.71(19)

[a] BS1, 6-31G(d); BS2, Lanl2DZ for Co and 6-31G(d) for remaining atoms; BS3, 6-31+G(d) for Co and 6-31G(d) for remaining atoms.

tional and electronic spectrum were carried out. The prominent absorption bands were assigned and main electron excitation transitions were investigated.

Experimental and Computational Section

According to a previously reported procedure,[17] the self-assembled $(CoL)_2$ complex (Figure 1) was synthesized and characterized by ^1H and ^{13}C NMR spectroscopy and mass spectrometry.

1. Spectroscopy. The FT-Raman spectra of $(CoL)_2$ complex was recorded in the solid powder with an IFS 120HR spectrometer equipped with an integrated FRA 106 (Bruker) Raman module. The 1064 nm radiation from a Nd:YAG laser was used for excitation. A laser power of 500 mW was selected. A high-sensitivity Ge detector was used, and each spectrum represented 700 scans. The spectra resolution was 4 cm^{-1} and the region of interest was 3600−100 cm^{-1}. The FT-IR spectra were measured with a 170SX FT-IR spectrometer (Nicolet) in KBr tablets, and the spectral range was 4000−400 cm^{-1}.

2. Calculations. Becke's[29a−d] 1988 exchange functional in combination with Becke's three-parameter hybrid exchange functional using the LYP[29e] correlation functional of Lee, Yang, and Parr (B3LYP) was employed in the DFT calculations. The ground-state geometry was optimized in the gas phase without any symmetry constraint. Three kinds of basis sets [BS1, 6-31G(d) for all elements; BS2, LanL2DZ for cobalt atom and 6-31G(d) for the remaining atoms; BS3, 6-31+G(d) for cobalt atom and 6-31G(d) for remaining atoms] were employed for comparison on the geometrical optimization. Analytical vibration frequencies were calculated at B3LYP/BS1 and B3LYP/BS2 levels of theory on optimized geometry. Time-dependent density functional theory (TD-DFT) excited-state calculations were determined at the B3LYP/BS2//B3LYP/BS2 level of theory in both the gas phase and CH_2Cl_2 solution. A polariable continuum model (PCM) with inclusion of solvent effect was employed and CH_2Cl_2 was selected as solvent in excitation energy calculations. The lowest 70 spin-allowed singlet transitions were investigated to simulate the absorption spectrum. DFT and TDDFT calculations were performed using the Gaussian 03 software package.[30] Although TDDFT calculations does not provide the electronic structures of excited states, the electronic distributions and localizations of the singlet excited-state may be visualized using the electron density difference maps (EDDMs).[31] GaussSum 1.03[32] was used for singlet EDDMs calculation and for the simulation of the vibrational and electronic spectrum.

Results and Discussion

1. Geometries. The structure and the numbering of atoms for $(CoL)_2$ is shown in Figure 1. Single crystal XRD shows that the molecular structure of complex adopts double-stranded helical geometry. The central Co(II) atom is tetracoordinated with four N-atoms from two distinct ligand with distorted tetrahedron geometry. In Table 1, optimized geometrical parameters under C_1 symmetry of $(CoL)_2$ by three kinds of basis sets [BS1, 6-31G(d) for all elements; BS2, LanL2DZ for cobalt atom and 6-31G(d) for the remaining atoms; BS3, 6-31+G(d) for cobalt atom and 6-31G(d) for other atoms] are compared to the available X-ray experimental data.[17] We notice that although the Co−N distances optimized using the mixed basis sets (BS2 and BS3) are slightly more accurate than those obtained with 6-31G(d) (BS1), for the optimized bond angles three types of

TABLE 2: Calculated Vibrational Wavenumbers at B3LYP/BS1 and B3LYP/BS2 Levels of Theory in the Gas Phase and Measured IR and Raman Band Positions (cm^{-1}) and Assignments for $(CoL)_2$ Complex[a]

	B3LYP/BS1			B3LYP/BS2			observed			
assign.[b]	freq [c]/cm^{-1}	IR intensity[d]	Raman activity	freq [c]/cm^{-1}	IR intensity	Raman activity	IR	Raman	$(ZnL)_2$[33]	NiOEP[34]
υ(=C_m−H)	3023	5.1	102.8	3026	20.1	126.0		3013	3027	3041
υ_{as}(CH_3)	2960	26.8	143.9	2960	22.6	148.6		2961		
υ_{as}(CH_3)	2955	64.2	258.4	2955	77.6	128.9	2949		2949	
υ_s(CH_3)	2916	53.4	919.2	2916	65.4	719.9		2912	2922	
υ_s(CH_3)	2915	102.4	130.2	2914	95.1	972.7	2905			
υ_s(CH_3)	2879	95.1	474.4	2881	102.4	130.2	2858		2853	
υ(C=O)	1757	484.3	31.2	1757	513.5	30.8	1738			
υ(C_α−C_m)	1596	650.3	217.5	1597	723.7	108.1	1596		1603	1603
υ(C_α−C_m)	1594	14.66	1213	1595	565.9	9.3		1595		
υ(C_β−C_β)	1509	113.7	27.1	1511	127.9	26.3	1532	1547	1567	1577
δ_{as}(CH_3)	1454	0.5	307.0	1453	19.7	181.9		1451	1456	
δ_{as}(CH_3)	1456	28.0	15.5	1456	28.8	9.6	1440		1435	
υ(pyr.half-ring)$_{sym}$	1345	24.0	6579.6	1348	26.3	7070.3	1390	1384	1386	1393
υ(pyr.half-ring)$_{sym}$	1338	104.9	6868.4	1342	218.7	3645.9	1365			1383
ω(CH_2)	1288	282.1	34.8	1286	221.3	22.8	1295			
δ(C_m-H)	1232	221.8	65.5	1231	209.2	79.2	1223	1238		1231,1220
υ_{asym}(C_β - C)	1159	300.1	16.4	1160	307.4	14.4	1163	1161	1162	1058
υ(pyr.half-ring)$_{asym}$	1107	4.4	170.3	1112	25.4	45.8		1115	1105	1121
υ(pyr.half-ring)$_{asym}$	1082	82.5	15.1	1081	67.4	21.2	1099			
υ(C−O)	1054	148.4	27.7	1054	141.7	39.4	1045			
ρ(CH_3)	1023	41.8	4.5	1023	32.9	20.8	1018			
ρ(CH_3)	1008	25.1	674.3	1008	18.9	543.9		1003		
υ(C−C)	952	87.9	11.8	955	78.7	2.6	962		981	
δ(pyr.def)$_{asym}$	915	54.2	3.8	914	38.2	3.4	920			927
γ(C_m−H)	892	1.0	1338.2	890	7.9	641.4		897		
γ(C_m−H)	846	138.0	141.9	846	160.4	103.0	850		854	
υ(C−C)	772	34.4	5.4	768	36.6	32.6	781			
ρ(CH_2)	741	2.3	25.3	738	2.0	18.1	734			
δ(pyr def)$_{sym}$	704	62.2	37.1	702	64.7	45.5	710	706	693	674
out-of-plane def of pyrrole	665	38.0	4.4	666	31.6	5.7	662	654	658	
δ(pyr rot.)	548	11.5	45.2	549	4.8	33.5	566			551
δ(pyr rot.)	527	18.8	58.7	527	11.1	71.3	534	529	513	544
δ(C_β−C−C_β)	450	16.3	16.7	453	15.0	2.4	478			
δ(C_β−C−C_β)	418	4.1	423.5	412	3.1	180.6		407		
υ(Co−N)	366	4.1	437.1	359	7.2	308.9		353		
υ(Co−N)	246	1.3	161.9	233	3.8	185.3		228		
δ(pyr transl)	152	2.8	57.0	152	2.3	47.5		134	118	144

[a] BS1, 6-31G(d); BS2, LanL2DZ for Co atom and 6-31G(d) for remaining atoms. [b] Abbreviations and symbols: asym, asymmetric; sym, symmetric; pyr, pyrrole; def, deformation; rot., rotation; transl, translation; υ, stretch; δ, bending; ω, out-of-plane wagging. [c] Scaled by 0.9614. [d] IR intensity: KM mol^{-1}. Raman activity: A**4/AMU.

basis sets give comparable values. The BS2 produces a comparable accuracy to BS3 but spends less computation time, so it is used for calculating the IR, Raman, and UV−vis absorption spectrum of $(CoL)_2$. The calculated Co−N bond lengths are slightly shorter than XRD experimental values. In detail, the Co−N bond lengths obtained with 6-31G(d) basis set are shorter by 0.054−0.077 Å than the XRD experimental bond lengths. When the Lanl2dz basis set and effective core potential (ECP) are used for the cobalt atom (BS2), the Co−N bonds are elongated by 0.015−0.031 Å but are still shorter by 0.027−0.055 Å than experimental bond lengths. The bond lengths optimized with 6-31+G(d) basis set (BS3) are comparable to those with the Lanl2dz basis set. From Table 1, we can find that large derivations appear on bond angles. The most significant differences in geometry are found for N6−Co1−N1, N4−Co2−N7, N5−Co1−N1, and N4−Co2−N8 bond angles, and the absolute errors are 23.6°, 25.9°, 10.0°, and 13.4°, respectively.

2. Vibrational Spectrum. The vibrational wavenumbers and IR, Raman intensities of $(CoL)_2$ were calculated at B3LYP/BS1 and B3LYP/BS2 levels of theory, respectively, at the optimized geometry. It is known that ab initio and DFT potentials systematically overestimate the vibrational wavenumbers. These discrepancies can be corrected by directly scaling the calculated values with a proper factor. In the present work, all calculated harmonic wavenumbers are scaled by a common factor of 0.9614. According to the calculated vibrational wavenumbers, IR and Raman intensities, and the normal-mode analysis, the prominent absorption bands are then assigned (Tables 2). To explore the effect of substituent on the characteristic skeletal vibrational modes of bis(dipyrrin), the FT-IR and Raman spectra of $(ZnL')_2$[33] (L′ = bis(2,4-dimethyldipyrrin-3-yl) methane) and NiOEP[34] are also presented in Tables 2.

The $(CoL)_2$ has 172 atoms and will produce 510 normal vibration modes. At the optimized structure of $(CoL)_2$, no imaginary wavenumber modes were obtained, proving that a true minimum on the potential energy surface was found. Comparing the scaled wavenumbers with the experimental fundamentals, B3LYP along with BS1 and BS2 reproduced well the experimental spectra, and the deviations are typically less than 30 cm^{-1}. The solid-state FT-IR and Raman spectral of $(CoL)_2$ as well as the simulated spectra in the gas phase are presented together in Figures 2 and 3. The vibrational eigenvectors related to some of the strongest IR and Raman bands

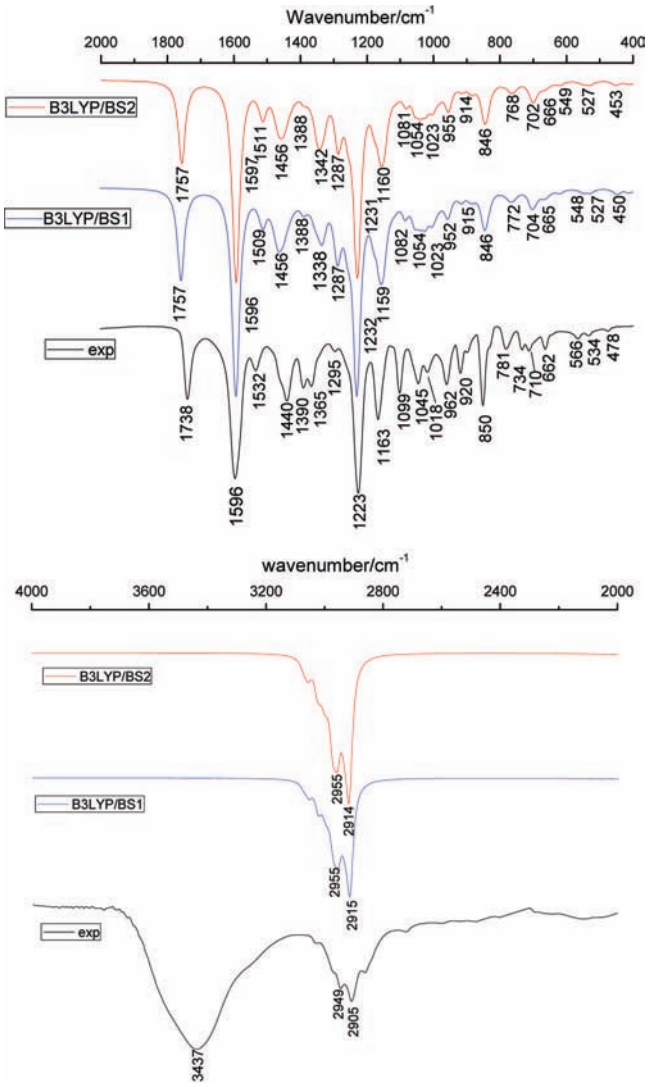

Figure 2. FT-IR spectrum (in KBr tablets) and calculated spectrum of $(CoL)_2$ in the gas phase using B3LYP with different combined basis sets [BS1, 6-31G(d); BS2, LanL2DZ for Co atom and 6-31G(d) for remaining atoms].

are shown in the Supporting Information. Comparing the IR and Raman spectrum calculated at the B3LYP/BS1 level with those calculated at the B3LYP/BS2 level, we can find that BS1 reproduces almost the same spectrum as BS2. The slight difference in geometry does not make prominent changes on the vibrational wavenumber and intensity. As for the same normal mode, the shift is within 6 cm^{-1}.

The normal-mode analysis and the experimental spectrum show that the characteristic skeletal vibrational modes of the pyrrole ring are presented in the IR and Raman spectra of $(CoL)_2$ as well as of $(ZnL')_2$ and NiOEP. As with the same vibrational modes, the shifts in wavenumbers are within 20 cm^{-1}.

A broad and strong band locating at 3407 cm^{-1} is the characteristic absorption band for water. The peak at 3013 cm^{-1} in the Raman spectrum is assigned to the mode $\upsilon(=C_m-H)$, but the same vibrational mode cannot be observed in the IR and simulated spectrum. The asymmetric and symmetric stretching vibrational mode of methyl appears at 2949, 2905, and 2858 cm^{-1} in the IR spectrum and at 2912 cm^{-1} in the Raman spectrum. A very strong band in the IR spectrum at 1738 cm^{-1} is identified as the stretching vibration of carbonyl in the $COOCH_3$ group. The computed value for this mode is 1757 cm^{-1}. The strongest band in the IR spectrum can be seen at 1596 cm^{-1}, and NMA reveals it arises from the stretching mode of $C_\alpha-C_m$. The corresponding mode can be observed at 1595 cm^{-1} in the Raman spectrum. Theoretical calculations reproduce well its position and intensity. A very weak band at 1532 cm^{-1} in the IR spectrum and at 1547 cm^{-1} in the Raman spectrum is assigned to the stretching vibration of $C_\beta-C_\beta$.The symmetric stretching vibration of pyrrole half-ring appears as weak shoulder bands at 1390 and 1365 cm^{-1} in the IR spectrum and a strong band at 1384 cm^{-1} in the Raman spectrum. DFT calculations underestimate these two bands by 27−45 cm^{-1}. The asymmetric stretching vibration of the pyrrole half-ring appears at 1099 cm^{-1} in the IR spectrum and at 1115 cm^{-1} in the Raman spectrum. The bending vibration mode of C_m-H appears as a very strong band located at 1223 cm^{-1} in the IR spectrum and DFT calculations predict accurately its wavenumber and intensity. (The calculated wavenumber is 1231 cm^{-1} and its intensity is 221.8 KM mol^{-1}). The asymmetric and symmetric bending vibration of pyrrole represents as weak bands at 920 and 710 cm^{-1} in the IR spectrum and at 706 cm^{-1} in the Raman spectrum. The out-of-plane deformation of pyrrole ring occurs at 662 cm^{-1} in the IR spectrum and at 654 cm^{-1} in the Raman spectrum. The asymmetric stretching vibration of $C_\beta-C$ can be observed at 1163 cm^{-1} in the IR spectrum and at 1161 cm^{-1} in the Raman spectrum. The band arising from out-of-plane deformation of C_m-H is found at 850 cm^{-1} in the IR spectrum, and the corresponding Raman band is identified at 897 cm^{-1}. Insertion of a metal ion in the center of the molecule results in some new vibrational modes. The Co−N stretching vibration can be observed at 353 and 228 cm^{-1} in the Raman spectrum. Comparison of vibrational spectrum between $(CoL)_2$ and $(ZnL')_2$ shows that the substitution of methyl on C_β atom results in significant wavenumber shifts on the same modes, particularly in the case of mode $\upsilon(C_\beta-C_\beta)$. As for $(CoL)_2$, the $C_\beta-C_\beta$ stretching vibration can be observed at 1532 and 1547 cm^{-1} in the IR spectrum; however, the corresponding mode can be observed at 1567 cm^{-1} in the IR spectrum of $(ZnL')_2$; the wavenumber shift is about 20 cm^{-1}. The wavenumber shifts of other modes are found to be within 10 cm^{-1}.

3. Electronic Structure. It will be useful to examine the nature of the frontier molecular orbitals for $(CoL)_2$ to provide the framework for the excited-state TDDFT calculation in the next section. A schematic representation of the energy level for $(CoL)_2$ calculated with BS1, BS2, and BS3 basis sets in the gas phase, respectively, is reported in Figure 4. A detailed analysis of several frontier molecular orbital compositions is presented in Table 3. The energy level of HOMO and LUMO are prominently higher or lower than that of HOMO−1 and LUMO+1. $(CoL)_2$ has pseudo-C_2 symmetry; the HOMO−1 and HOMO−2, HOMO−3, and HOMO−4 are degenerate in energy. The energy levels of HOMO−6, HOMO−7, and HOMO−8 are very close and slightly lower than that of HOMO−5. As it can be noticed from Figure 4, enlarging the basis set from BS1 to BS3 does not lead to sizable changes in the energy and character of the frontier orbitals. The HOMO−LUMO energy gap is 0.42, 0.41, and 0.41 eV for BS1, BS2, and BS3, respectively.

The highest occupied molecular orbitals (HOMOs) can be divided into three subgroups. The HOMO have essentially cobalt d orbital (d_{xy}) character (67%) with sizable contribution coming from the bis(bipyrrin-3-yl)methane orbitals (30%), mixed in an antibonding fashion with a metal states. The HOMO−5 to HOMO−8, HOMO−14, and HOMO−16 represents the bonding counterpart of HOMO, corresponding to the combination

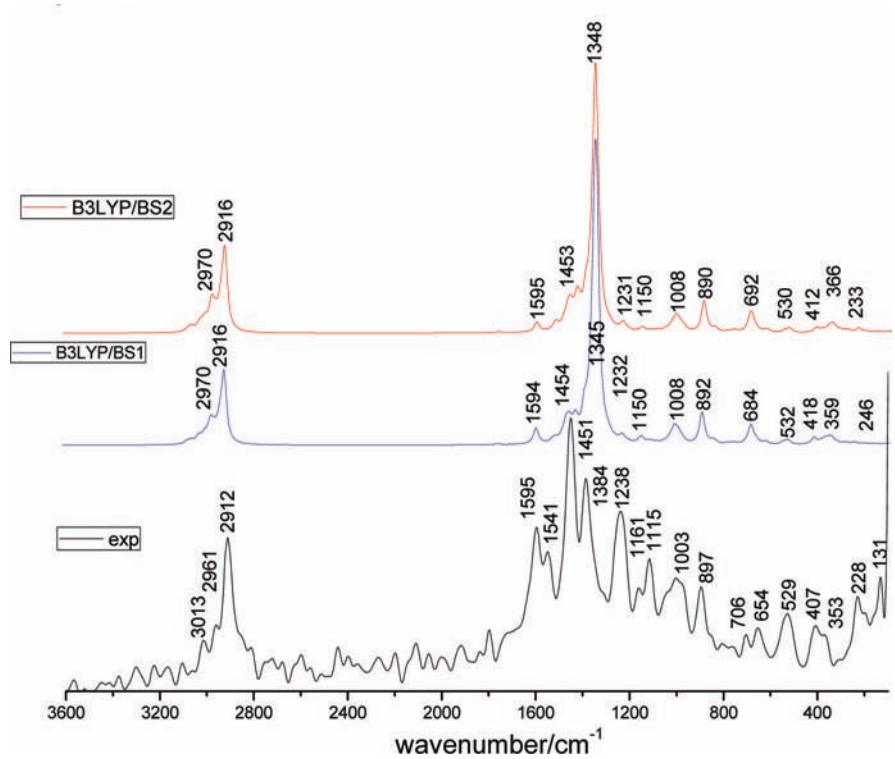

Figure 3. FT-Raman spectrum (in powder) and calculated spectrum of $(CoL)_2$ in the gas phase using B3LYP with different basis sets [BS1, 6-31G(d); BS2, LanL2DZ for Co atom and 6-31G(d) for remaining atoms].

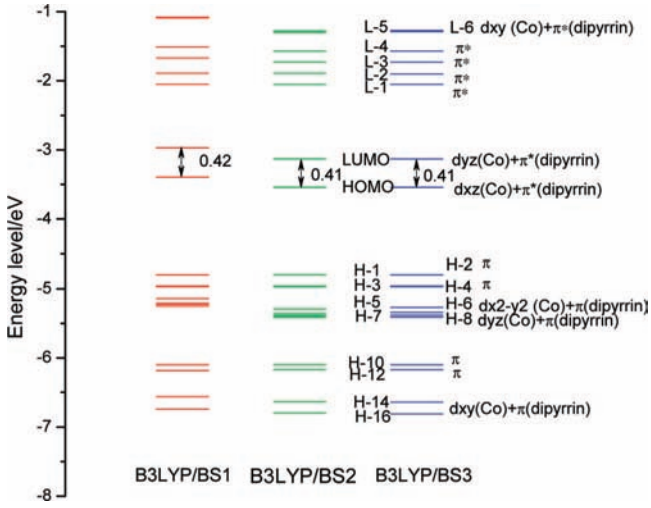

Figure 4. Frontier molecular orbital energy level (eV) and main characters of $(CoL)_2$ calculated in gas phase using B3LYP with different basis sets [BS1, 6-31G(d); BS2, Lanl2DZ for Co atom and 6-31G(d) for remaining atoms; BS3, 6-31+G(d) for Co atom and 6-31G(d) for remaining atoms].

between the cobalt d orbital and the dipyrrin π orbitals. The HOMO−1 to HOMO−4, HOMO−10, and HOMO−12 are combined π bonding orbitals localized on the bis(bipyrrin-3-yl)methane. See the Supporting Information.

The lowest unoccupied molecular orbital (LUMOs) are also classified as two types. One type is π^* orbitals localized on the bis(dipyrrin-3-yl)methane ligand, with slight contribution from cobalt atoms, and the other are antibonding combinations of the cobalt d oribtials with the bis(bipyrrin-3-yl)methane π orbitals. LUMO+1 to LUMO+4 have prominent contribution from two bis(dipyrrin-3-yl)methane ligand (total 85%) and 9−12% contribution from cobalt atom. LUMO, LUMO+5, and LUMO+6 have 66% contribution from cobalt d orbital and total 32% contribution from bis(dipyrrin-3-yl)methane ligand. They are antibonding combinations of the cobalt d oribtials and dipyrrin ring π^* orbitals.

4. UV−Vis Absorption Spectrum. In the range of 425−625nm, the experimental spectrum of $(CoL)_2$ shows two main features,[17] labeled as I and II, in order of increase energy. The very strong absorbance band I centered at 525.5 nm (2.36 eV) is followed at higher energy by the medium strong band II centered at 488.1 nm (2.54 eV). The 70 singlet→singlet spin-allowed excited states up to an energy of about 3.42 eV were calculated by using the method of TDDFT. Only the electronic transitions, whose oscillator strength value (*f*) are higher than 0.1, are reported. The vertical excitation energy and oscillator strength along with the main excitation configuration are summarized in Table 4. To check how reasonable the calculations results results were, the absorption spectrum of $(CoL)_2$ was simulated on the basis of the calculations. Each excited state was interpolated by Gaussian convolution with the full width at half-maximum (fwhm) of 1000 cm^{-1}. The simulated spectrum is listed in the Supporting Information. Two overlapped bands are found with intensity maximums at 534 nm (3.22 eV) and 442 nm (3.80 eV), respectively. It is obvious that positions of the two band maximums in the observed spectrum are well-described in the simulated spectrum. However, their relative intensity is not very consistent with the experimental data. Contrary to the experimental information, the simulated band I is much lower than band II.

Considerable configuration mixings is found for a number of transitions. In TD/B3LYP calculation, 24^1A excited-state calculated at 535.5 nm has an oscillator strength of 0.1405 and is comparable to the experimental band I. In the excitation, the H−1→L+1 configuration has the largest coefficient (70%) in CI wave functions and is responsible for this absorption. As shown in Table 3, the HOMO−1 orbital has its primary contribution from the delocalized π orbital of bis(dipyrrin-3-

TABLE 3: Percentage Composition of the Lowest Unoccupied and Highest Occupied Orbitals of the Complex $(CoL)_2$ in Terms of Cobalt, Bis(dipyrrin-3-yl)methane, and Substituent

		composition %					
MO	energy/eV	Co	BD_1[a]	BD_2	CH_3	$COOCH_3$	assignment of orbital
L+6	−1.27	66	16	16	1	1	d_{xy}(Co) + π*(dipyrrin)
L+5	−1.29	66	16	15	1	1	d_{xy}(Co)+π*(dipyrrin)
L+4	−1.57	10	42	43	4	1	π*(dipyrrin)
L+3	−1.73	11	42	42	4	1	π*(dipyrrin)
L+2	−1.9	12	41	41	6	0	π*(dipyrrin)
L+1	−2.05	9	43	42	6	0	π*(dipyrrin)
LUMO	−3.13	66	15	16	3	0	d_{xz}(Co) + π*(dipyrrin)
HOMO	−3.54	67	15	15	3	0	d_{xz}(Co)+π*(dipyrrin)
H−1	−4.8	0	87	6	5	1	π(dipyrrin)
H−2	−4.8	0	6	87	5	1	π(dipyrrin)
H−3	−4.96	0	25	67	6	1	π(dipyrrin)
H−4	−4.97	0	67	26	6	1	π(dipyrrin)
H−5	−5.27	45	25	26	4	0	$d_{x^2-y^2}$(Co) + π(dipyrrin)
H−6	−5.34	49	25	23	3	1	$d_{x^2-y^2}$(Co) + π(dipyrrin)
H−7	−5.38	54	20	22	2	2	d_{yz}(Co) + π(dipyrrin)
H−8	−5.41	53	21	22	3	2	d_{yz}(Co) + π(dipyrrin)
H−10	−6.1	7	43	42	6	1	π(dipyrrin)
H−12	−6.17	11	39	39	5	5	π(dipyrrin)
H−14	−6.64	55	21	20	3	0	d_{xy}(Co) + π(dipyrrin)
H−16	−6.81	54	22	20	4	0	d_{xy}(Co) + π(dipyrrin)

[a] BD: bis(dipyrrin-3-yl)methane.

TABLE 4: Computed Excitation Energies (EE), Oscillator Strengths (f), and Electronic Transition Configurations (contribution > 10%) for the Optical Transitions with f > 0.1 for Complex $(CoL)_2$ in the Gas Phase and in CH_2Cl_2 Solution

		TD-B3LYP/BS2[a]				PCM-TD-B3LYP/BS2 (in CH_2Cl_2)				
exp[17]	states	EE/eV	f	configuration	main attrib	states	EE/eV	f	configuration	main attrib
I 525.5 (2.36)	24^1A	535.5 (2.32)	0.1405	H−1→L+1 (70%) H−10→LUMO (−10%)	$\pi\rightarrow\pi$*	24^1A	536.5 (2.31)	0.2001	H−1→L+1 (54%) H−2→L+1 (21%)	$\pi\rightarrow\pi$*
	44^1A	443.7 (2.79)	0.1839	H−12→LUMO (22%) H−2→L+3 (−11%) H−1→L+3 (−20%)	MLCT/$\pi\rightarrow\pi$*	44^1A	445.7 (2.78)	0.2419	H−12→LUMO(+31%) H−2→L+3(19%) H−16→LUMO(+11%)	MLCT/$\pi\rightarrow\pi$*
II 488.1 (2.54)	45^1A	442.0 (2.81)	0.1276	H−5→L+1 (17%) H−5→L+2 (23%) H−2→L+3 (10%)	MLCT/$\pi\rightarrow\pi$*	45^1A	444.1 (2.79)	0.4108	H−1→L+3 (+22%) H−2→L+3 (18%)	$\pi\rightarrow\pi$*
	46^1A	440.6 (2.81)	0.2045	H−6→L+1 (−11%) H−5→L+2 (−23%) H−2→L+3 (23%)	MLCT/$\pi\rightarrow\pi$*	48^1A	431.5 (2.87)	0.1004	H−6→L+2 (−16%) H−3→L+3 (18%)	MLCT/$\pi\rightarrow\pi$*
	60^1A	398.4 (3.11)	0.5819	H−4→L+4 (47%)	$\pi\rightarrow\pi$*	60^1A	401.7 (3.09)	0.5331	H−4→L+4 (56%)	$\pi\rightarrow\pi$*
	64^1A	387.2 (3.20)	0.2797	no major configuation	MLCT	63^1A	392.4 (3.16)	0.4367	H−14→LUMO (11%)	MLCT

[a] BS2 is LanL2DZ for Co atom and 6-31G(d) for remaining atoms.

yl)methane [BD_1 (87%) and BD_2 (6%)], and the LUMO+1 orbital is the π* orbital delocalized over two bis(dipyrrin-3-yl)methane ligands (BD_1 43%, BD_2, 42%). It is indicated as a $\pi\rightarrow\pi$* transition. The electron density redistribution in 24^1A excited-state is presented in the Supporting Information. The red and green colors show the regions of increased and decreased electron density, respectively. Alternative appearance of green and red color region over two bis(dipyrrin-3-yl)methane ligands proves further the 24^1A exited state mainly originates from ligand $\pi\rightarrow\pi$* transition. For the band II centered at 488.1 nm, the 44^1A, 45^1A, and 46^1A excited states have significant oscillator strengths and correspond to this absorption. The initial states are HOMO−5, HOMO−6, and HOMO−12 orbitals, which have sizable contributions of metal Co 3d orbitals mixed with dipyrrin ring character, and the final states are LUMOs primarily contributed from dipyrrin ring π* orbitals. A metal-to-ligand charge transfer (MLCT) transition is indicted. Moreover, it also involves transition from the H−1, H−2, and H−3 orbitals, with primary contribution of dipyrrin ring, to the unoccupied dipyrrin ring π* orbitals. Thus, a MLCT mixed with ligand $\pi\rightarrow\pi$* transition is suggested for the band II. The electron density distribution map (EDDM) of 44^1A and 45^1A (see Supporting Information) reveal further a mixture of MLCT and ligand $\pi\rightarrow\pi$* transitions.

Though the simulated spectrum of $(CoL)_2$ in the gas phase has given a reasonable agreement on the band maximum positions with the experiment results, calculations including solvent effect are carried out with the expectation of a better match-up between the simulated and the experimental results. On the basis of the optimized geometry in the gas phase, the lowest 70 singlet→singlet spin-allowed excited states up to an energy of about 3.25 eV are obtained by the application of TDDFT in combination with PCM to reproduce a solvent effect. Each excited-state has also been interpolated by a Gaussian convolution with the fwhm of 1000 cm^{-1}. The simulated spectrum in solution is also shown in the Supporting Information with two maximum bands centered at 534 nm (2.32 eV) and 444 nm (2.79 eV), respectively. Contrary to the expectation, the simulated spectrum with inclusion of the solvent effect does not brings a better match-up result to the experimental. PCM model provides a comparable accuracy on excitation energy and oscillator strengths to TDDFT in the gas phase.

Excitation energies, oscillator strengths, and corresponding transitions compositions for the two simulated absorption bands in CH_2Cl_2 solution are reported in Table 4. For the band I, the initial states are still HOMO−1 and HOMO−2 orbitals, which have primary contribution from delocalized π orbital of bis-(dipyrrin-3-yl)methane, and the final states are LUMO+1,

primarily contributed from the dipyrrin ring π^* orbital. An interligand $\pi \rightarrow \pi^*$ transition is also indicated. For band II, a MLCT mixed with ligand $\pi \rightarrow \pi^*$ transition is also suggested. The involved transitions primitively come from the cobalt 3d orbital to the dipyrrin rings π^* orbitals. Moreover, it also involves transitions from HOMO−1, HOMO−2, and HOMO−3 orbitals, with the primary contribution of the dipyrrin ring to the unoccupied dipyrrin ring π^* orbital. The above analysis reveals that the transition mechanisms for the two simulated bands in CH_2Cl_2 solution are similar to that in the gas phase.

Conclusions

A combined experimental and computational study of a large self-assembly complex $(CoL)_2$ containing 172 atoms was reported. An extensive DFT and time-dependent DFT study of this complex in the gas phase and in CH_2Cl_2 solution was performed, investigating the effect of substitutions of methyl and methyl propionate on the electronic structure and optical properties of this complex. The calculated IR and Raman spectra are in excellent agreement with the experiment, thus allowing a detailed assignment of the vibrational absorption bands. Comparing the vibrational spectrum of $(CoL)_2$ with that of $(ZnL')_2$, the substitution of methyl on the C_β atom results in sizable shifts on the same modes; particularly in the case of mode $\upsilon(C_\beta-C_\beta)$, the shift is more than 20 cm^{-1}. The lowest 70 singlet−singlet spin-allowed excitation states were taken into account for the calculation by TDDFT in the gas phase and PCM-TDDFT in CH_2Cl_2 solution. Theoretical calculations provide a good description of positions of the two band maximums in the observed spectrum but predict a contrary relative intensity for these two bands. In the UV−vis absorption spectrum of $(CoL)_2$ complex, the band maximum centered at 525.5 nm is mainly attributed to the $\pi \rightarrow \pi^*$ transition. The band maximum centered at 488.1 nm originated from the MLCT transition mixed with the ligand $\pi \rightarrow \pi^*$ transition.

Acknowledgment. This work is supported by the National Natural Science Foundation of China, contract/grant number: 20701030; Foundation of Hubei Provincial Department of Education, contract/grant number: Q200717002; the Young People Project of Wuhan Science and Technology Bureau, contract/grant No. 200850731380; Foundation of Wuhan Universtiy of Science and Engineering, contract/grant number: 20063103; Project of China National Textile And Apparel Council, contract/grant number: 2007052; Natural Science Foundation of Hubei Province contract/grant number: 2005ABA016.

Supporting Information Available: Vibrational eigenvectors relevant to the strongest IR and Raman bands, isodensity plots of the frontier orbitals (isovalue = 0.02) of $(CoL)_2$ in CH_2Cl_2 solution, the simulated UV−vis absorption spectrum of $(CoL)_2$ calculated by TDDFT in the gas phase and by PCM-TDDFT in CH_2Cl_2 solution using B3LYP/BS2//B3LYP/BS2, and changes of electron density distribution between the 24^1A, 44^1A, and 45^1A excited states and the ground state of $(CoL)_2$. This information is available free of charge via the Internet at http://pubs.acs.org.

References and Notes

(1) Piguet, C.; Bernardinelli, G.; Hopfgartner, G. *Chem. Rev.* **1997**, *97*, 2005.
(2) Weissbuch, I.; Cohen, S.; Cohen, H.; Leiserowitz, L.; Lahav, M.; Kjaer, K.; Howes, P. B.; Als-Nielsen, J.; Lehn, J. M.; Baxter, P. N. W.; Hanan, G., S.; Schubert, U. S. *J. Am. Chem. Soc.* **1998**, *120*, 4850.
(3) Fujita, M.; Su, S. Y.; Kusukawa, T.; Funaki, H.; Ogura, K.; Yamaguchi, K. *Angew. Chem., Int. Ed.* **1998**, *37*, 2082.
(4) Baxter, P. N.; Hanan, G. S.; Lehn, J. M. *Chem. Commun.* **1996**, *17*, 2019.
(5) Funeriu, D. P.; Lehn, J. M.; Baum, G.; Fenske, D. *Chem.-Eur. J.* **1997**, *3*, 99.
(6) Halper, S. R.; Cohen, S. M. *Chem. Eur. J.* **2003**, *9*, 4661.
(7) Halper, S. R.; Cohen, S. M. *Inorg. Chem.* **2005**, *44*, 486.
(8) Thoi, V. S.; Stork, J. R.; Magde, D.; Cohen, S. M. *Inorg. Chem.* **2006**, *45*, 10688.
(9) Bacchi, A.; Carcelli, M.; Gabba, L.; Ianelli, S.; Pelagatti, P. *Inorg. Chim. Acta* **2003**, *342*, 229.
(10) Yilmaz, M. D.; Bozdemir, O. A.; Akkaya, E. U. *Org. Lett.* **2006**, *8*, 2871.
(11) Blakemore, J. D.; Chitta, R.; D'Souza, F. *Tetrahedron Lett.* **2007**, *48*, 1977.
(12) Maeda, H.; Hasegawa, M.; Hashimoto, T.; Kakimoto, T.; Nishio, S.; Nakanishi, T. *J. Am. Chem. Soc.* **2006**, *128*, 10024.
(13) Wu, Z. K.; Chen, Q. Q.; Xiong, S. X.; Xin, B.; Zhao, Z. W.; Jiang, L. J.; Ma, J. S. *Angew. Chem., Int. Ed.* **2003**, *42*, 3271.
(14) Zhang, Y.; Wang, Z. M.; Yan, C. H.; Li, G. P.; Ma, J. S. *Tetrahedron Lett.* **2000**, *41*, 7717.
(15) Chen, Q. Q.; Zhang, Y. J.; Dolphin, D. *Tetrahedron Lett.* **2002**, *43*, 8413.
(16) Yang, L. Y.; Chen, Q. Q.; Yang, G. Q.; Ma, J. S. *Tetrahedron* **2003**, *59*, 10037.
(17) Yang, L. Y.; Zhang, Y.; Yang, G. Q.; Chen, Q. Q.; Ma, J. S. *Dyes Pigm.* **2004**, *62*, 27.
(18) Yu, L. H.; Muthukumaran, K.; Sazanovich, I. V.; Kirmaier, C.; Hindin, E.; Diers, J. R.; Boyle, P. D.; Bocian, D. F.; Holten, D.; Lindsey, J. S. *Inorg. Chem.* **2003**, *42*, 6629.
(19) D'Souza, F.; Smith, P. M.; Zandler, M. E.; McCarty, A. L.; Itou, M.; Araki, Y.; Ito, O. *J. Am. Chem. Soc.* **2004**, *126*, 7898.
(20) Wong, M. W. *Chem. Phys. Lett.* **1996**, *256*, 391.
(21) Bytheway, I.; Wong, M. W. *Chem. Phys. Lett.* **1998**, *282*, 219.
(22) Vlček, A., Jr.; ZáliŠ, S. *Coord. Chem. Rev.* **2007**, *251*, 258.
(23) Ciofini, I.; Lainé, P. P.; Bedioui, F.; Adamo, C. *J. Am. Chem. Soc.* **2004**, *126*, 10763.
(24) Nazeeruddin, M. K.; Angelis, F. D.; Fantacci, S.; Selloni, A.; Viscardi, G.; Liska, P.; Ito, S.; Takeru, B.; Grätzel, M. *J. Am. Chem. Soc.* **2005**, *127*, 16835.
(25) Miao, T. F.; Li, S.; Cai, J. *J. Mol. Struct. (THEOCHEM)* **2008**, *855*, 45.
(26) Xu, L. C.; Li, J.; Shi, S.; Zheng, K. C.; Ji, L. N. *J. Mol. Struct. (THEOCHEM)* **2008**, *855*, 77.
(27) Li, M. X.; Zhou, X.; Xia, B. H.; Zhang, H. X.; Pan, Q. J.; Liu, T.; Fu, H. G.; Sun, C. C. *Inorg. Chem.* **2008**, *47*, 2312.
(28) David, K. S.; Hemeryck, A.; Tancrez, N.; Toupet, L.; Williams, J. A. G.; Ledoux, I.; Zyss, J.; Boucekkine, A.; Guégan, J. P.; Bozec, H. L.; Maury, O. *J. Am. Chem. Soc.* **2006**, *128*, 12243.
(29) (a) Becke, A. D. *J. Chem. Phys.* **1993**, *98*, 5648. (b) Becke, A. D. *Phys. Rev. A* **1988**, *38*, 3098. (c) Becke, A. D. *J. Chem. Phys.* **1993**, *98*, 1372. (d) Vosko, S. H.; Wilk, L.; Nusair, M. *Can. J. Phys.* **1980**, *58*, 1200. (e) Lee, C.; Yang, W.; Parr, P. G. *Phys. Rev. B* **1988**, *37*, 785.
(30) Frisch, M. J.; et al. *Gaussian 03*; Gaussian, Inc.: Pittsburgh, PA, 2003.
(31) Browne, W. R.; O'Boyle, N. M.; McGarvey, J. J.; Vos, J. G. *Chem. Soc. Rev.* **2005**, *34*, 641.
(32) O'Boyle ; N. M., Vos, J. G. *GaussSum 1.0*; Dublin City University, 2005. Available at http://gausssum.sourceforge.net.
(33) Li, W.; Wang, Y. B.; Yang, L. Y.; Shang, X. F.; Cai, X.; Szeghalmi, A.; Ye, Y.; Ma, J. S.; Luo, M. D.; Hu, J. M.; Kiefer, W. *J. Phys. Chem. B* **2006**, *110*, 21958.
(34) Li, X. Y.; Czernuszewicz, R. S.; Kincaid, J. R.; Su, Y. O.; Spiro, T. G. *J. Phys. Chem.* **1990**, *94*, 31.

JP808793S